HHS Public Access

Author manuscript

Opt Lett. Author manuscript; available in PMC 2013 September 26.

Published in final edited form as:

Opt Lett. 2013 August 1; 38(15): 2683–2686.

Random-access optical-resolution photoacoustic microscopy using a digital micromirror device

Jinyang Liang, **Yong Zhou**, **Amy W. Winkler**, **Lidai Wang**, **Konstantin I. Maslov**, **Chiye Li**, and **Lihong V. Wang***

Optical Imaging Laboratory, Department of Biomedical Engineering, Washington University in St. Louis, Campus Box 1097, One Brookings Drive, St. Louis, Missouri 63130, USA

Abstract

We developed random-access optical-resolution photoacoustic microscopy using a digital micromirror device. This system can rapidly scan arbitrarily shaped regions of interest within a 40×40 μm^2 imaging area with a lateral resolution of 3.6 μm. To identify a region of interest, a global structural image is first acquired, then the selected region is scanned. The random-access ability was demonstrated by imaging two static samples, a carbon fiber cross and a monolayer of red blood cells, with an acquisition rate up to 4 kilohertz. The system was then used to monitor blood flow *in vivo* in real time within user-selected capillaries in a mouse ear. By imaging only the capillary of interest, the frame rate was increased by up to 9.2 times.

Optical-resolution photoacoustic microscopy (OR-PAM) [1,2] has been widely used in various biomedical applications [3–6] to provide functional, structural, and molecular images *in vivo* [7]. The scanning mechanism has always been a major research interest in OR-PAM because fast scanning speed and flexible scanning access are desired to monitor physiological dynamics with high temporal resolution. The scanning speed of OR-PAM has been improved by using several devices, including a high-speed voice-coil stage [8], a water-immersible MEMS scanning mirror [9], and an ultrasonic array transducer with multifocal optical illumination [10].

A variety of physiological dynamics, such as microvascular blood flow and neural signal transition, occurs in micrometer-scale spatial structures (e.g., capillaries and dendritic spines) with irregular shapes. To acquire these time-dependent processes at high frame rates, it is desired to conduct measurements on user-selectable regions of interest. In previous approaches, however, the laser focus of OR-PAM needs to be raster-scanned continuously for every successive scan, which limits the scanning speed.

The capability of scanning only user-selectable regions of interest, termed random-access scanning, has been realized in other imaging modalities, such as fluorescent two-photon or multi-photon microscopy, by using galvanometers or acousto-optic deflectors (AODs) [11,12]. Galvanometers provide random access scanning rates only in the kilohertz range.

*Corresponding author: LHWANG@WUSTL.EDU.

AOD-based scanning can be extremely fast. However, it has to be tuned to a particular optical wavelength range, which complicates multi-wavelength operation (such as sO_2 measurements) in PAM.

A digital micromirror device [13] is another candidate to realize random-access scanning. As a widely used spatial light modulator, it provides flexible and high-speed control of optical patterns that are delivered to the target. It has been implemented in many optical imaging modalities, such as confocal microscopy [14,15], hyperspectral imaging [16], and fluorescence imaging [17,18].

In this letter, we present a random-access OR-PAM (RA-OR-PAM) system using a digital micromirror device (DMD). Because the micromirrors are independently controlled, regions of interest with arbitrary user-selected shapes can be imaged without redundancy. The laser beam exclusively scans these regions, resulting in faster successive scans. The DMD device supports a scanning rate of up to 20 kHz, enabling a system frame rate equal to 20 kHz divided by the number of desired pixels. The high temporal resolution of RA-OR-PAM supports high-speed structural and functional imaging and enables photoacoustic monitoring of dynamic physiological processes *in vivo*.

The RA-OR-PAM system (Fig. 1) employs a diode- pumped solid-state laser (INNOSLAB, Edgewave, $\lambda = 532$ nm) as the illumination source. This laser has maximum output pulse energy of 300 μJ. Although it can operate at a repetition rate up to 30 kHz, 20 kHz is used to match the scanning rate of the DMD. The laser beam first passes through a spatial filtering stage and is expanded to a 15-mm-diameter collimated beam that matches the DMD size. The DMD (Texas Instrument, Discovery 4100) consists of a 1024×768 array of 13.68×13.68 μm^2 micromirrors. To realize the “ON” and “OFF” states, each micromirror can be latched in two positions, at ±12° from the DMD surface normal. When the expanded laser beam is oriented toward the DMD surface at approximately 24°, “ON” pixels diffract light toward the microscope, while the “OFF” pixels diffract light toward a beam stop. The photoacoustic (PA) signal is detected by a 50 MHz, spherically focused (numerical aperture (NA) = 0.5) ultrasound transducer (V214-BB-RM, Olympus NDT Panametrics) confocal with the objective lens. For each laser pulse, a one-dimensional depth-resolved image (A-line) is obtained by recoding the time-to-flight PA signal. A volumetric image of the target’s optical absorption is produced by two-dimensional optical scanning with the DMD. The volumetric 3-D images can be rendered as 2-D maximum amplitude projection (MAP) images along the depth direction. The imaging system consists of two 4-*f* telescopes with a total magnification ratio of 263:1. The DMD surface (768×768 micromirrors) is imaged to within a 40×40 μm^2 square, such that the full DMD scanning area is within the acoustic focus of the ultrasound transducer.

The system can operate in either global raster scanning or random-access scanning mode. To increase the optical fluence on the object without damaging the DMD, a single imaging pixel is illuminated with 96×96 micromirror pixels, referred to hereafter as a super-pixel. The scanning step size is 1/4 of a super-pixel, or 24 micromirrors. Therefore, each global raster scan has a total of 841 pixels. User-selected regions of interest can be subsequently scanned in random-access scanning mode. A regional structural image is reconstructed by

allocating the acquired photoacoustic signals to the corresponding pixels within the selected regions of interest. In addition, functional images may be acquired at very high frame rates when the areas of the regions of interest are much smaller than the global scanning area.

In order to compensate for the spatial non-uniformity of the optical fluence and acoustic detection sensitivity, the system was calibrated using a thin square chromium target made in-house by vacuum-deposition on a microscope coverslip substrate. The chromium target was thin compared to the acoustic resolution yet optically thick, such that it exhibited a uniform photoacoustic signal. Also, the square edges achieved by photo-resist masking were verified with scanning electron microscopy to be sharp in comparison to the optical wavelength. Because the super-pixel on the DMD was imaged, instead of focused, to the target, the lateral resolution of the RA-OR-PAM system depended upon the super-pixel size, the magnification ratio, and the system NA. The NA required to capture 83% of the optical energy from each super-pixel was 0.11, which was much smaller than the NA of the objective lens. Therefore, the lateral resolution was mainly determined by the imaged super-pixel size. Alternatively, one can consider that the effective NA of the objective lens is 0.11, which limited the lateral resolution. Correspondingly, an objective lens with NA $\approx$ 0.11 could be used to receive 83% of the optical energy. However, the truncation of 17% of the optical energy would cause a small loss of resolution. Such a loss can be avoided by using an objective lens with a greater NA.

The lateral resolution of the RA-OR-PAM was quantified by imaging the sharp edge of a square. A maximum amplitude projection (MAP) image is shown in Fig. 2 (a). The edge spread function (ESF) was calculated by averaging along each line parallel to the x-axis (Fig. 2 (b)). Taking the derivative of the ESF yielded the line spread function (LSF, Fig. 2(c)), which was further interpolated with cubic spline. The lateral resolution as defined by the full-width-half-maximum (FWHM) of the interpolated LSF was 3.6 μm.

We first tested the system by imaging a carbon-fiber cross. The target was first imaged using global raster scanning (Fig. 3(a)) with a frame rate of 23.8 Hz. Regions of interest were identified and imaged using random access scanning. The specific regions included a 5-point cross pattern, the central row of the horizontal fiber, and cross sections of the two fibers on both ends (Fig. 3 (b)–(d)). The first pattern can be potentially applied to record the calcium transition in neural dendrites [11], while the other two patterns are useful for measuring blood flow velocity in capillaries [8]. Based on the size of the regions of interest with respect to the global scanning area, the random-access scanning increased the image acquisition speed by 168.2×, 29.0× and 31.2×, corresponding to frame rates of 4003.2 Hz (Fig. 3 (b)), 690.4 Hz (Fig. 3 (c)), and 742.4 Hz (Fig. 3 (d)), respectively. The high scanning frequency made this system well suited for obtaining functional images of fast time-dependent physiological processes.

To test the RA-OR-PAM system performance with biological contrasts, we imaged red blood cells (RBCs). A monolayer RBC target was prepared by spreading a drop of the whole bovine blood across a thin cover glass. Global raster scanning (Fig. 4 (a)) showed that sparsely distributed RBCs could be clearly distinguished. Three RBCs on the upper-right part of the image were selected as the regions of interest. Random-access scanning (Fig. 4

(b)) successfully reconstructed these selected RBCs with a scanning speed enhanced by13.6×.

To demonstrate the advantage of RA-OR-PAM, we imaged capillaries in a nude mouse ear (Hsd:Athymic Nude-Foxn1^{nu}, Harlan Co.) to monitor physiological dynamics *in vivo*. The global raster scanning provided structural images with clearly resolved capillaries. Two selected capillary features are shown in Fig. 5. The time- resolved acoustic detection enabled us to distinguish two crossed capillaries separated by approximately 9 μm along the depth direction (Fig. 5 (a)). In addition, we captured RBC clusters flowing along both capillaries in real-time video (Fig. 5 (b)). In another capillary feature, the RBC clusters flowed through a loop capillary with a bifurcation on the left (Fig. 5 (c)). Images of single RBCs were captured when this loop capillary became clogged; subsequent reperfusion was observed at a higher-than-average blood flow speed (Fig. 5 (d)).

Random-access scanning was implemented for the loop capillary (Fig. 6 (a,b)) and a capillary bifurcation (Fig. 6 (c,d)). As with the global structural images, we were able to capture flowing RBC clusters in these selected capillaries. The random-access scanning speeds were 6.0× and 9.2× faster, respectively, as compared to global raster scanning. All experimental animal procedures were conducted in conformance with the laboratory animal protocol approved by the Animal Studies Committee of Washington University in St. Louis.

In summary, we have demonstrated a DMD-based RA-OR-PAM system capable of volumetric global and regional structural imaging with a 3.6 μm lateral resolution. Random-access scanning significantly increased the scanning speed within user-selected regions of interest, making this system a promising tool to investigate time-dependent physiological processes *in vivo*. We envision that RA-OR-PAM will empower a variety of structural and functional imaging applications.

Acknowledgments

The authors thank the help of Dr. Liang Gao in the system design, and Professor James Ballard's close reading of the manuscript. This work was sponsored in part by National Institutes of Health grants DP1 EB016986 (NIH Director's Pioneer Award), R01 EB008085, R01 CA134539, U54 CA136398, R01 EB010049, R01 CA157277, and R01 CA159959. L.W. has a financial interest in Microphotoacoustics, Inc. and Endra, Inc., which, however, did not support this work. K.M. has a financial interest in Microphotoacoustics, Inc., which, however, did not support this work.

References

1. Maslov K, Zhang HF, Hu S, Wang LV. Optical-resolution photoacoustic microscopy for in vivo imaging of single capillaries. Opt Lett. 2008; 33:929–931. [PubMed: 18451942]
2. Hu S, Maslov K, Wang LV. Second-generation optical-resolution photoacoustic microscopy with improved sensitivity and speed. Opt Lett. 2011; 36:1134–1136. [PubMed: 21479007]
3. Jiao S, Jiang M, Hu J, Fawzi A, Zhou Q, Shung KK, Puliafito CA, Zhang HF. Photoacoustic ophthalmoscopy for in vivo retinal imaging. Opt Express. 2010; 18:3967–3972. [PubMed: 20389409]
4. Wang L, Maslov K, Wang LV. Single-cell label-free photoacoustic flowoxigraphy in vivo. Proceedings of the National Academy of Sciences. 2013

5. Paproski RJ, Forbrich AE, Wachowicz K, Hitt MM, Zemp RJ. Tyrosinase as a dual reporter gene for both photoacoustic and magnetic resonance imaging. Biomed Opt Express. 2011; 2:771–780. [PubMed: 21483602]
6. Li R, Slipchenko MN, Wang P, Cheng JX. Compact high power barium nitrite crystal-based Raman laser at 1197 nm for photoacoustic imaging of fat. Journal of Biomedical Optics. 2013; 18:040502–040502. [PubMed: 23536057]
7. Wang LV, Hu S. Photoacoustic Tomography: In Vivo Imaging from Organelles to Organs. Science. 2012; 335:1458–1462. [PubMed: 22442475]
8. Wang L, Maslov K, Yao J, Rao B, Wang LV. Fast voice-coil scanning optical-resolution photoacoustic microscopy. Opt Lett. 2011; 36:139–141. [PubMed: 21263479]
9. Yao J, Huang CH, Wang L, Yang JM, Gao L, Maslov KI, Zou J, Wang LV. Wide-field fast-scanning photoacoustic microscopy based on a water-immersible MEMS scanning mirror. Journal of Biomedical Optics. 2012; 17:080505–080501. [PubMed: 23224156]
10. Li G, Maslov KI, Wang LV. Reflection-mode multifocal optical-resolution photoacoustic microscopy. Journal of Biomedical Optics. 2013; 18:030501–030501. [PubMed: 23446704]
11. Duemani Reddy G, Kelleher K, Fink R, Saggau P. Three-dimensional random access multiphoton microscopy for functional imaging of neuronal activity. Nat Neurosci. 2008; 11:713–720. [PubMed: 18432198]
12. Salomé R, Kremer Y, Dieudonné S, Léger JF, Krichevsky O, Wyart C, Chatenay D, Bourdieu L. Ultrafast random-access scanning in two-photon microscopy using acousto-optic deflectors. Journal of Neuroscience Methods. 2006; 154:161–174. [PubMed: 16458361]
13. Dudley D, Duncan WM, Slaughter J. Emerging digital micromirror device (DMD) applications. Proc SPIE. 2003; 4985:14–25.
14. Lane PM, Dlugan ALP, Richards-Kortum R, MacAulay CE. Fiber-optic confocal microscopy using a spatial light modulator. Opt Lett. 2000; 25:1780–1782. [PubMed: 18066342]
15. Hanley, Verveer; Gemkow, J Arndt; Jovin. An optical sectioning programmable array microscope implemented with a digital micromirror device. Journal of Microscopy. 1999; 196:317–331. [PubMed: 10594772]
16. Saint-Cyr M, Lakhiani C, Cheng A, Mangum M, Liang J, Teotia S, Livingston EH, Zuzak KJ. In-vivo quantitative evaluation of perfusion zones and perfusion gradient in the deep inferior epigastric artery perforator flap. Proc SPIE. 2013; 8618:861806–861806.
17. Studer V, Bobin J, Chahid M, Mousavi HS, Candes E, Dahan M. Compressive fluorescence microscopy for biological and hyperspectral imaging. Proceedings of the National Academy of Sciences. 2012; 109:E1679–E1687.
18. Kocabas A, Shen CH, Guo ZV, Ramanathan S. Controlling interneuron activity in Caenorhabditis elegans to evoke chemotactic behaviour. Nature. 2012; 490:273–277. [PubMed: 23000898]

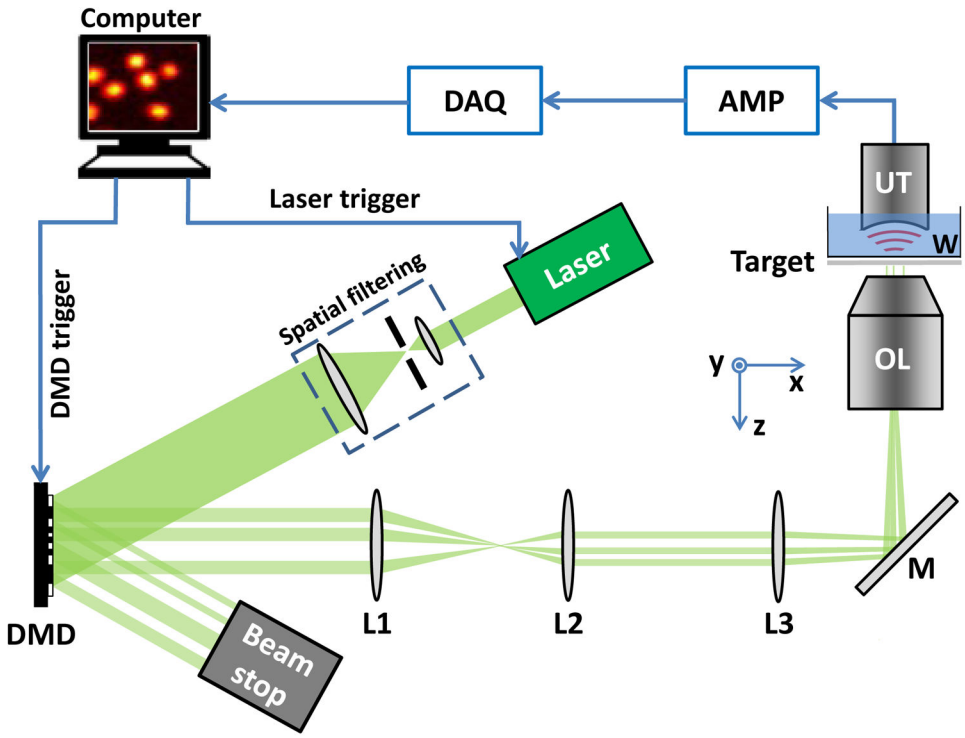

Fig. 1.

Schematic overview of the RA-OR-PAM system, not to scale. AMP, signal amplifiers and filters; DAQ, data acquisition; DMD, digital micromirror device; L1–L3, lenses (focal lengths: f_1 = 100 mm, f_2 = 30 mm, and f_3 = 160 mm); M, mirror; OL, Objective lens (Olympus, 100×, NA 1.4 oil-immersion); UT, ultrasound transducer; W, water.

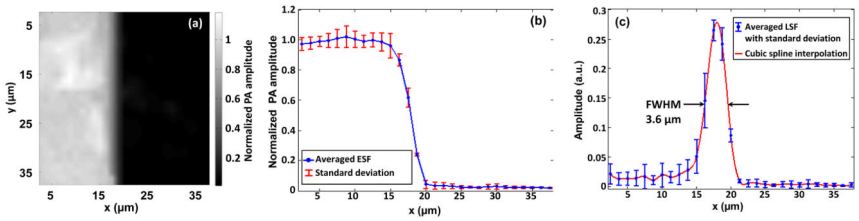

Fig. 2.

Quantification of the lateral resolution of the RA-OR-PAM system. (a) PA image of an edge made of deposited chromium. (b) Edge spread function (ESF) extracted from (a). (c) Line spread function (LSF) extracted from (b) and interpolated with cubic spline.

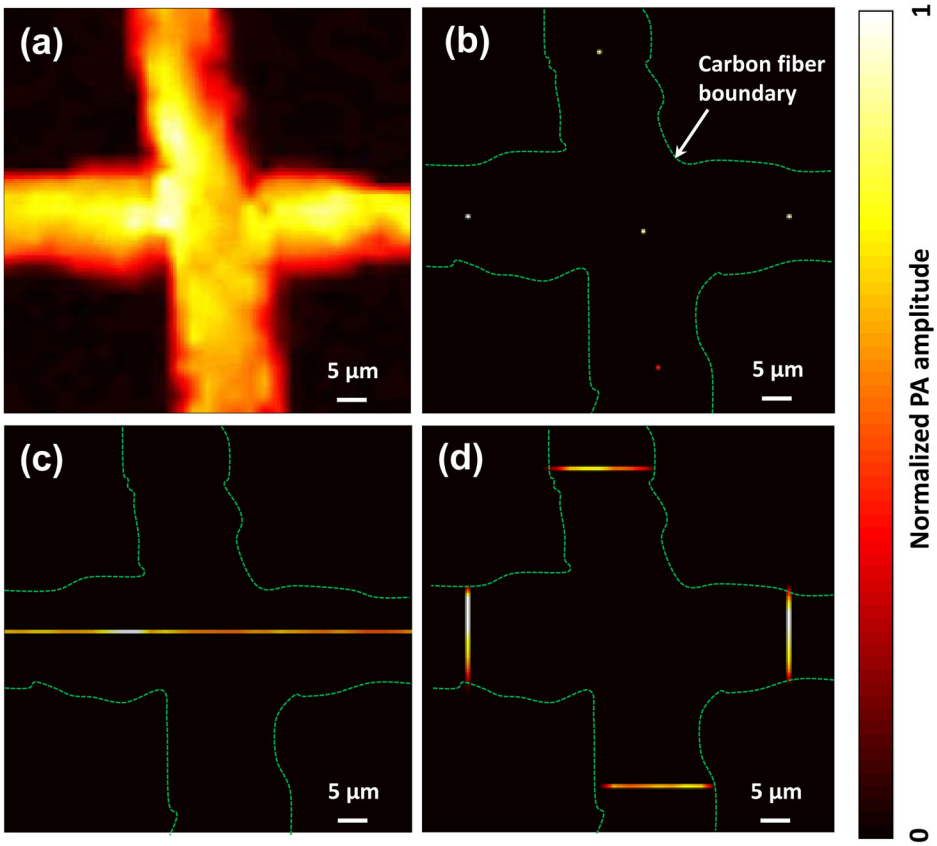

Fig. 3.

PA images of a carbon-fiber cross acquired using four scanning methods: (a) global raster scanning, (b) 5-point cross pattern, (c) central row of the horizontal fiber, and (d) cross sections on the two fibers on both ends. The entire scanning area is 40×40 μm^2.

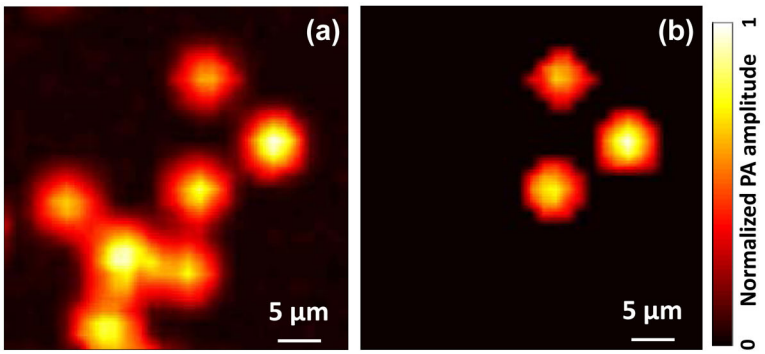

Fig. 4.

PA imaging of a monolayer of red blood cells (RBC) using (a) global raster scanning and (b) random-access scanning. The entire scanning area is 40×40 μm^2.

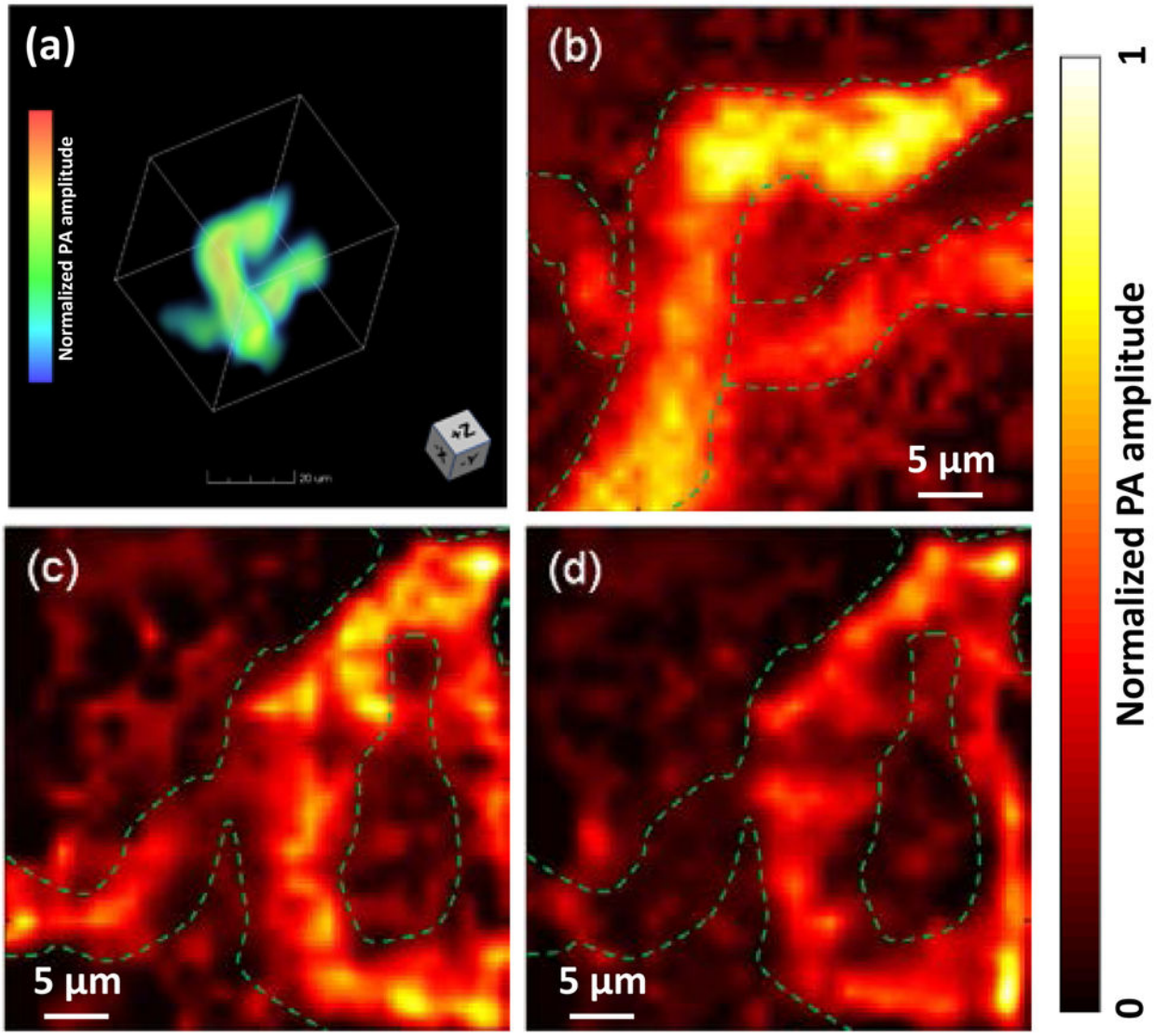

Fig. 5.

Real-time imaging of capillary features and blood flow dynamics in a mouse ear *in vivo*. (a) 3-D view of two crossed capillaries at different depths (Media 1), (b) flow dynamics of the structure in (a) (Media 2), (c) RBC clusters flowing through a loop capillary with a bifurcation (Media 3), and (d) capillary clogging and reperfusion (Media 4).

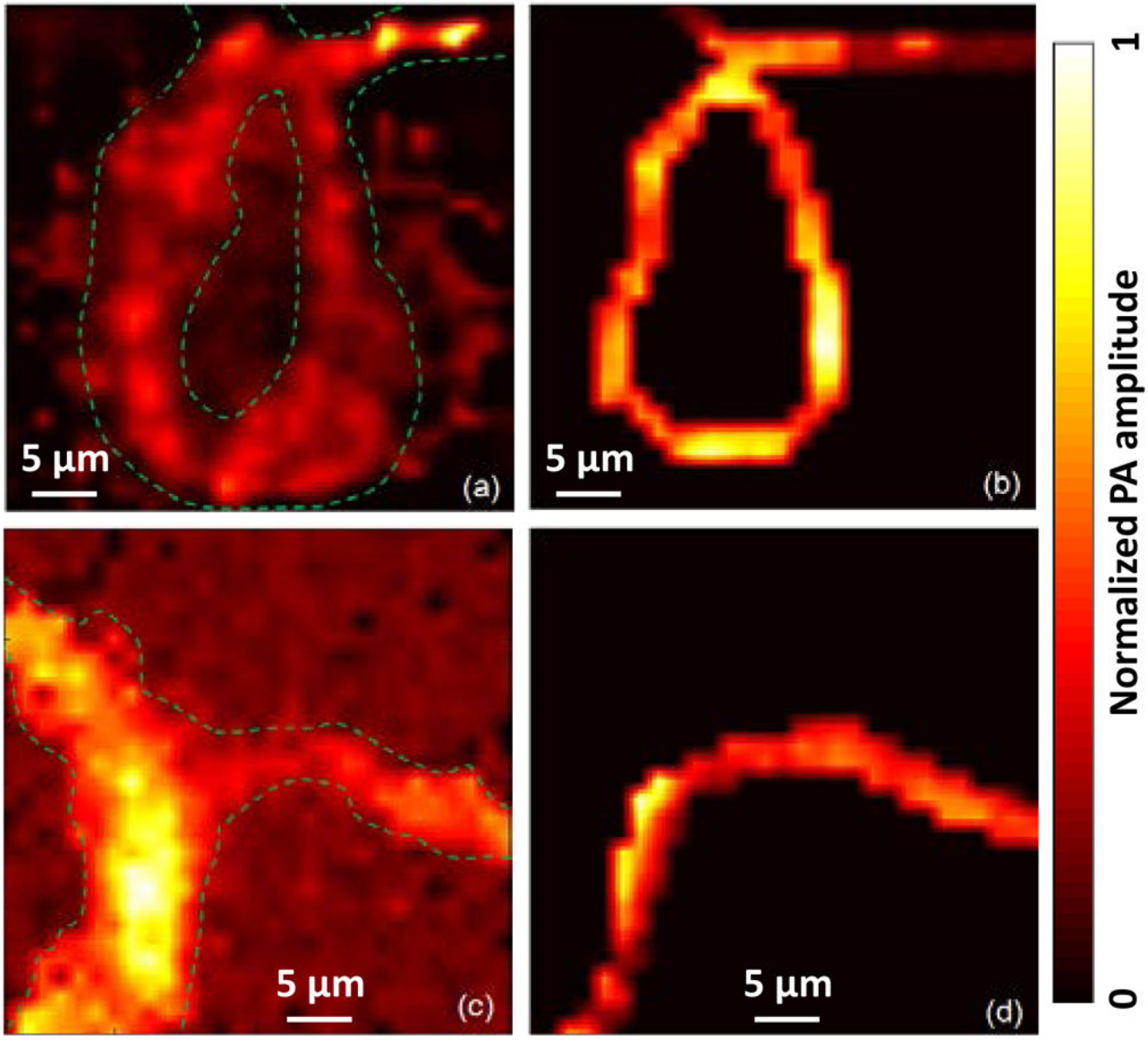

Fig. 6.

Real-time imaging of blood flow in a mouse ear in a loop capillary *in vivo* using (a) global raster scanning (Media 5) and (b) random-access scanning (Media 6). A capillary bifurcation was also imaged using (c) global raster scanning (Media 7) and (d) random-access scanning (Media 8).